

Spring constant calibration of atomic force microscopy cantilevers with a piezosensor transfer standard

E. D. Langlois^{a)}

Materials Science & Engineering Laboratory, National Institute of Standards & Technology, Boulder, Colorado 80305, USA and Department of Mechanical Engineering, University of Colorado, Boulder, Colorado 80309, USA

G. A. Shaw, J. A. Kramar, and J. R. Pratt

Manufacturing Engineering Laboratory, National Institute of Standards & Technology, Gaithersburg, Maryland 20899, USA

D. C. Hurley^{b)}

Materials Science & Engineering Laboratory, National Institute of Standards & Technology, Boulder, Colorado 80305, USA

(Received 10 August 2007; accepted 27 August 2007; published online 24 September 2007)

We describe a method to calibrate the spring constants of cantilevers for atomic force microscopy (AFM). The method makes use of a “piezosensor” composed of a piezoresistive cantilever and accompanying electronics. The piezosensor was calibrated before use with an absolute force standard, the NIST electrostatic force balance (EFB). In this way, the piezosensor acts as a force transfer standard traceable to the International System of Units. Seven single-crystal silicon cantilevers with rectangular geometries and nominal spring constants from 0.2 to 40 N/m were measured with the piezosensor method. The values obtained for the spring constant were compared to measurements by four other techniques: the thermal noise method, the Sader method, force loading by a calibrated nanoindentation load cell, and direct calibration by force loading with the EFB. Results from different methods for the same cantilever were generally in agreement, but differed by up to 300% from nominal values. When used properly, the piezosensor approach provides spring-constant values that are accurate to $\pm 10\%$ or better. Methods such as this will improve the ability to extract quantitative information from AFM methods. © 2007 American Institute of Physics. [DOI: 10.1063/1.2785413]

I. INTRODUCTION

The power of atomic force microscopy (AFM) has grown dramatically since its inception two decades ago. One area of current emphasis lies in extracting quantitative information about materials properties with AFM and related methods. Applications span a wide range of systems, from single molecules to biological materials to engineering thin films. (For a review, see, for instance, Ref. 1.) Common to all applications is the use of nano- and picoscale forces. Therefore, in order to better exploit AFM and its offshoots for quantitative information, we must improve our ability to accurately measure and control forces on these very small scales.

The force F applied by the tip of the AFM cantilever is usually not measured directly. Instead, it is inferred from the relationship $F = k_C \delta_C$, where δ_C is the cantilever deflection measured by the AFM photodiode sensor and k_C is the cantilever spring constant or stiffness. Accurate measurement of AFM forces thus hinges on accurate knowledge of the cantilever spring constant. However, processing variations during cantilever fabrication mean that the nominal values of k_C provided by manufacturers can vary dramatically—

sometimes more than 100%—from the actual value for a specific cantilever. Thus, it becomes imperative to directly measure k_C for the particular cantilever in use.

Here, we describe a method to calibrate the spring constants of AFM cantilevers by means of a piezoresistive cantilever. The cantilever and its accompanying electronics form a “piezosensor” whose voltage depends on the applied force. Before use, the response of the piezosensor was calibrated with an absolute force standard in order to create a force transfer standard. We show how the piezosensor method can be used to measure cantilevers with a wide range of spring constants and compare the results to values obtained by four other methods.

II. CREATING A FORCE TRANSFER STANDARD

Use of a piezoresistive cantilever to determine cantilever spring constants is one form of the so-called reference cantilever or cantilever-on-cantilever method. In this method, a test cantilever with unknown k_C is brought into contact with a second cantilever (or other device) with known stiffness. The test cantilever’s deflection relative to that of the reference cantilever leads to a determination of k_C . This basic method has been implemented a variety of ways, by means of both passive devices^{2–6} and active sensors.^{7–9}

^{a)}Present address: Analog Devices, Cambridge, MA 02139.

^{b)}Electronic mail: hurley@boulder.nist.gov

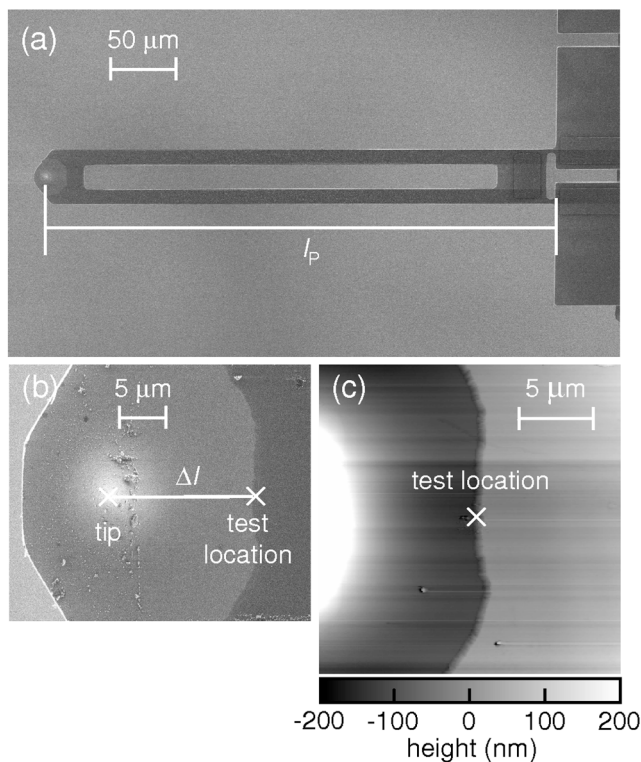


FIG. 1. Images of the piezoresistive cantilever used in the piezosensor force transfer standard. (a) SEM image of the cantilever in plan view. The distance from the tip to the clamped end of the cantilever is denoted by l_p . (b) SEM close-up of the tip region. The cross indicates the position at which the cantilever spring constant was measured. The distance between the tip and the point at which the measurements were made is denoted by Δl . (c) Example of AFM topography image obtained during a cantilever spring-constant measurement. Such images were used to reliably locate the precise test position.

When combined with the appropriate electronics, piezoresistive cantilevers constitute active sensing devices whose electrical output changes in direct response to the applied force. For brevity, we will refer to the combination of the piezoresistive cantilever and its electronics as a piezosensor. Active sensors have certain advantages for use in cantilever calibration, as discussed below. Like any reference cantilever, the response of the piezosensor must be calibrated before use. At NIST, we have access to an absolute force standard for calibration, that is, forces traceable to the International System of Units (SI). This procedure turns the piezosensor into a secondary force artifact or force transfer standard. If this force transfer standard is subsequently used to calibrate AFM cantilevers, an unbroken link to the SI is maintained.

A. Piezosensor

The piezoresistive cantilever and accompanying electronics used in this work were obtained commercially (FMT-400, Kleindiek Nanotechnik GmbH, Reutlingen, Germany).¹⁰ Detailed technical information about the cantilever was not available. Scanning electron microscope (SEM) images of the piezoresistive cantilever are shown in Figs. 1(a) and 1(b). The plan-view image in Fig. 1(a) reveals

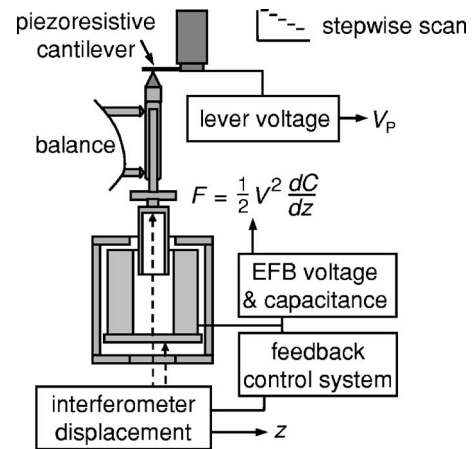


FIG. 2. Schematic of the electrostatic force balance (EFB) force standard used to calibrate the piezosensor transfer standard.

that the cantilever is approximately $400 \mu\text{m}$ long and $40 \mu\text{m}$ wide, with a slotted region along most of its length. SEM images in side view indicate that it is approximately $6 \mu\text{m}$ thick. When viewed from the side (not shown), the tip appears conical with a smoothly decreasing height. The SEM image in Fig. 1(b) shows a close-up of the end of the cantilever. Approximately $15 \mu\text{m}$ from the tip toward the clamped end of the cantilever, there is a sharp transition between the conical tip region and the flat body of the cantilever, created by the microfabrication process. The transition consists of a step approximately 200 nm high, as seen in the AFM topography image in Fig. 1(c). As discussed below, we made use of this step to reliably identify a measurement location.

For mounting, the piezoresistive cantilever is pressure fit into a metal harness with four contact clips. The cantilever, clips, and harness are integrated onto a small circuit board for ease of handling. The cantilever is mounted in the clips with its tip side facing upwards. The contact clips also establish electrical contact between the piezoresistive cantilever and its on-chip resistor and the rest of a Wheatstone resistance bridge. The resistance bridge (excitation voltage 2.5 V) converts changes in the cantilever resistance into changes in the output voltage V_p . The system electronics are housed in a separate unit that contains an amplifier and power supply in addition to the bridge circuit.

B. The NIST electrostatic force balance

At NIST, the primary standard for forces in the range 10^{-8} – 10^{-4} N is realized by use of an electrostatic force balance (EFB). Conceptually, this apparatus uses traceable measurements of distance, capacitance, and voltage to realize an electrostatic force traceable to SI units. Here, we briefly summarize the EFB apparatus and its principles of operation. A more detailed description is given elsewhere.¹¹

The key components of the EFB and its configuration for calibration of the piezosensor are shown in Fig. 2. The EFB is mounted inside a vacuum chamber and contains a coaxial cylindrical capacitor arrangement. Forces in the vertical (z) direction are generated when voltages are applied to the pair of nested, coaxial cylinders. The outer, high-voltage cylinder

remains fixed, and the inner, electrically grounded cylinder is free to move along the z -axis. In principle, the capacitance of this geometry varies linearly with the overlap between the two cylinders. If the cylinders are perfectly coaxial, the electric force is generated in the z -direction only. The inner cylinder is mounted in such a way that its motion is constrained to the z -axis and is relatively insensitive to any off-axis forces. Thus, the EFB generates an electrical force F along the balance axis that may be calculated from

$$F = \frac{1}{2} \frac{dC}{dz} V^2, \quad (1)$$

where V is voltage between the inner and outer electrodes and dC/dz is the capacitance gradient. The value for the gradient $dC/dz=0.9467$ pF/mm was determined in separate experiments in vacuum with a relative standard uncertainty of less than 10^{-4} .

C. Piezosensor calibration with the EFB

The EFB's traceable measurements of applied force and displacement enable direct calibration of the piezosensor traceable to the SI. To calibrate the piezosensor, the EFB was operated as an indenter. A conospherical indenter tip (radius $100 \mu\text{m}$, angle 90°) was attached to the moving arm of the balance and brought into contact with the piezoresistive cantilever. The indenter tip was positioned to contact the tip of the cantilever using a proximal microscope. The cantilever was mounted horizontally, so that the force applied by the indenter tip was normal to its long axis. During the approach, the balance was operated in displacement feedback control, and the balance setpoint was adjusted by $1 \mu\text{m}$ increments until contact was achieved. The point of contact was observed visually by an optical microscope with a long standoff distance. Contact was also determined by monitoring the output of the resistance bridge that had been nulled prior to contact. The initial contact load was estimated to be $3.5 \mu\text{N}$.

An automated routine was used to increment the balance setpoint and record the resulting force F , displacement z , and voltage V_p of the piezosensor. One loading cycle consisted of five equally spaced displacement values. It was found that the full range of the resistance bridge corresponded to approximately $10 \mu\text{m}$ of tip displacement. After the loading cycle, the balance setpoint was decremented over the same range in an unloading cycle. Measurements were obtained for 36 complete load/unload cycles over a force range of approximately $25 \mu\text{N}$.

With this procedure, two calibration parameters were determined: the sensitivity S and the spring constant k_p of the piezosensor. The sensitivity $S=dF/dV_p$ is the relationship between the applied force and the resulting output voltage V_p . The spring constant $k_p=dF/dz$ is the relationship between the applied force and the resulting deflection. Note that the values of k_p and S depend on the point of contact; this is discussed further below. The values $S=(24.58 \pm 0.14) \mu\text{N/V}$ and $k_p=(3.10 \pm 0.10) \text{N/m}$ were measured for the piezosensor.

III. MEASURING SPRING CONSTANTS WITH THE PIEZOSENSOR TRANSFER STANDARD

A. Experimental methods

Once the response of the piezosensor had been calibrated, it was used as a force transfer standard to determine the spring constant k_c of conventional AFM cantilevers. The experiments described below were performed on an MFP-3D instrument (Asylum Research, Santa Barbara, CA). The experimental procedure developed for this work used features of the MFP-3D that are not available on all commercial AFMs. Nonetheless, the general approach is broadly applicable and could be implemented on other AFMs with slight modifications.

For ease of use, the piezoresistive cantilever was mounted in a test fixture. The circuit board containing the cantilever and its wiring harness was attached to a glass microscope slide. Two spacers were placed between the circuit board and the slide to accommodate the deflection of the piezoresistive cantilever. The spacers were made from a ceramic oxide material due to its thermal stability and ease of machining. The resulting fixture was then placed on the sample stage of the AFM. The cantilever under test was mounted by standard methods in the AFM cantilever holder. The test fixture was aligned such that the long axis of the piezoresistive cantilever was parallel to that of the test cantilever, but with its tip end pointing in the opposite direction.

Measurement of the spring constant was begun by bringing the tip of the test cantilever in contact with the piezoresistive cantilever. The ideal point of contact is the end of the (upward-facing) tip of the piezoresistive cantilever, at the same spot at which the EFB calibration was performed. Such alignment is difficult to achieve in practice, however, and might damage one or both tips. Instead, we used another position on the piezoresistive cantilever that could be located relatively easily, reliably, and precisely. After the test cantilever was brought in contact, it was scanned in contact mode to obtain a topography image of the piezoresistive cantilever. One such topography image is shown in Fig. 1(c). The step transition between the conical tip region (left) and the flat body of the piezoresistive cantilever (right) is easy to identify. Immediately to the left of the step, the conical tip region is relatively flat. We chose a position close to the step as a reliable location to perform the calibration measurement. The distance between the tip of the piezoresistive cantilever and the step was measured by high-resolution SEM imaging [see Fig. 1(b)]. After the step was located by topography scanning, the tip of the test cantilever was positioned there by repeatedly decreasing the scan size. Topography scanning was also used to center the tip relative to the width of the piezoresistive cantilever. SEM images indicated that the height of the piezoresistive cantilever's tip was approximately $6 \mu\text{m}$. The nominal tip height for the test cantilevers was $10\text{--}20 \mu\text{m}$. Therefore, it is unlikely that the tip of the piezoresistive cantilever touched the underside of a test cantilever.

A custom subroutine for the AFM software platform was written to perform the calibration measurements. The subroutine was written with the IGOR PRO software package

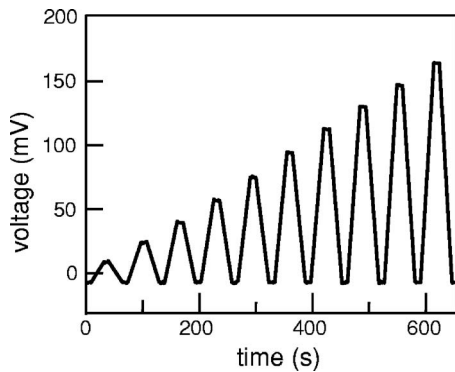


FIG. 3. Example of automated measurement for cantilever calibration. Shown is the voltage V_p output by the piezosensor as a function of time for a single test run. The z -scanner voltage was progressively increased in a series of ten steps, and the corresponding voltage of the piezosensor was measured. After each step, the system was returned to the preload condition in order to account for thermal and mechanical drift.

(WaveMetrics, Inc., Portland, OR). The subroutine applied a pattern of increasing voltage steps to the z -axis scanner in the AFM head. The resulting downward motion of the AFM head brought the two cantilevers together with increasing force, thus increasing the deflection of both cantilevers. Each step was preceded by a defined preload deflection and subsequently returned to that deflection before the next step. At the same time, the output voltage V_p of the piezosensor was recorded by the computer. With a data recording rate of 1 Hz, ten data points were acquired at each preload deflection and each step deflection. The process is illustrated in Fig. 3, which shows V_p as a function of time during one measurement. Care was taken to keep the cantilever deflection in the linear regime, according to $dy/dx = 3\delta/2l < 0.08$,¹² where dy/dx is the slope, δ is the deflection, and l is the length of the cantilever. A linear deflection condition ensures that any errors due to nonlinearities in the cantilever bending moment will be small (less than 1%).

During the measurement, the deflection of the test cantilever was controlled by a feedback loop that switched between the voltage of the position-sensitive photodiode detector and the voltage of the z -axis linear variable differential transformer (Z-LVDT) sensor. The photodiode voltage was used for closed-loop control of the preload deflection, and the Z-LVDT voltage was used for closed-loop control during the step deflection. This alternation was done for two reasons. First, closed-loop control with the Z-LVDT voltage gave greater mechanical stability between the two cantilevers, resulting in more stable values of the piezosensor's output voltage. Second, closed-loop control with the photodiode voltage for the preload was found to minimize mechanical drift of the AFM head. In addition, use of the Z-LVDT voltage for the closed-loop control avoids the inherent nonlinearity of the photodiode signal,^{13,14} so that a large total deflection with a linear step pattern can be achieved. The photodiode voltage was set at 0.01 V for the preload condition for all of the cantilevers measured. For each cantilever, the step pattern was divided into ten equal increments. The Z-LVDT incremental motion varied according to the stiffness of the specific test cantilever. The deflection increment needed for a particular cantilever to stay within

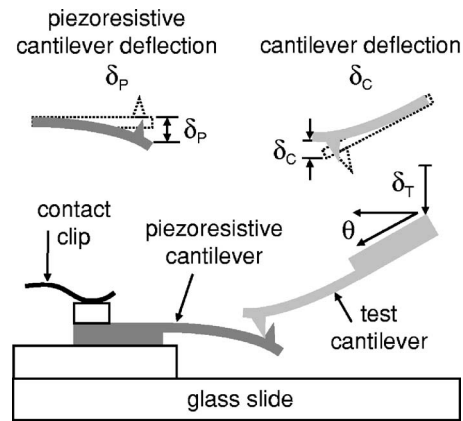


FIG. 4. Schematic of experimental configuration for calibration of AFM cantilevers with a piezosensor transfer standard.

the linear range of the photodiode was determined by testing prior to the calibration measurement.

After acquisition, the data were preprocessed as follows. Each set of ten data points for each preload and deflection step was averaged. The values of the preload deflection before and after each step deflection were averaged to obtain a baseline preload deflection voltage. The baseline value was then subtracted from the associated step deflection in order to obtain a value for the net deflection voltage ΔV_p . This process was intended to reduce the effects of any mechanical drift that occurred during a given step measurement. The software was programmed to perform the ramping process automatically ten times. In this way, the final output of the calibration measurement was ten sets of ten voltage points, for a total of 100 data points.

B. Data analysis

A second computer subroutine was written for data analysis. Figure 4 contains a diagram of the two-cantilever system and the variables involved. The spring constant of the test cantilever is denoted by k_{piezo} (that is, k_C as measured with the piezosensor). k_{piezo} is determined by¹⁵

$$k_{\text{piezo}} = F \cos^2 \theta / \delta_C, \quad (2)$$

where F is force in the z (vertical) direction, δ_C is the deflection of the test cantilever in the z direction, and θ is the tilt angle of the test cantilever with respect to horizontal. Based on the MFP-3D specifications, we used $\theta = 11^\circ$.

The force F is determined by

$$F = \Delta V_p S \zeta, \quad (3)$$

where ΔV_p is the net deflection voltage of the piezosensor and S is its sensitivity constant determined by the EFB calibration. The factor $\zeta = l_p / (l_p - \Delta l)$ accounts for the fact that the force is not applied at the same position on the piezoresistive cantilever as it was in the EFB calibration (see below). Here, l_p is the length of the piezoresistive cantilever from base to tip, and Δl is the distance between the tip and the point of contact with the test cantilever tip. These quantities are indicated in Fig. 1.

To determine the deflection δ_C of the test cantilever, conservation of z -displacement was used.⁹ Assuming that the

deformation of the test cantilever tip and the surface of the piezoresistive cantilever is negligible, the z -displacement obeys the relationship

$$\delta_T = \delta_C + \delta_P. \quad (4)$$

Here, δ_T is the total z -displacement of the AFM head measured by the Z-LVDT, and δ_C and δ_P are the z -deflection of the test cantilever and piezoresistive cantilever, respectively. The deflection δ_P of the piezoresistive cantilever is determined by

$$\delta_P = \frac{\Delta V_P S \zeta}{k_P \zeta^3} = \frac{\Delta V_P S}{k_P \zeta^2}, \quad (5)$$

where k_P is the spring constant of the piezoresistive cantilever determined by calibration with the EFB. The factor ζ denotes a “tip location coefficient.” As discussed above, the EFB calibration of the piezosensor was performed by applying the force to the tip of the piezoresistive cantilever. However, for practical reasons, the AFM cantilever calibrations were performed with their tips slightly closer to the base of the piezoresistive cantilever. This effectively stiffens the piezoresistive cantilever and reduces its deflection per applied force. For a perfectly rectangular piezoresistive cantilever, ζ is given by¹⁶

$$\zeta^3 = \frac{k_P + \Delta k}{k_P} = \left(\frac{l_P}{l_P - \Delta l} \right)^3. \quad (6)$$

Because k_P is multiplied by ζ^3 and hence depends on the third power of the difference in lengths, accurate knowledge of l_P and Δl is critical to achieve accurate values of k_C . This is one reason why the scanning procedure described above to position the test cantilever tip was developed. In our analysis, we used $l_P = (389.7 \pm 0.9) \mu\text{m}$ and $l_P - \Delta l = (374.4 \pm 0.9) \mu\text{m}$, so that $\zeta = 1.041 \pm 0.004$. The values of l_P and $l_P - \Delta l$ were obtained by calibrated length measurements in SEM images similar to those shown in Fig. 1(a). The actual value of ζ for our piezoresistive cantilever may differ from the assumed value. Equation (6) applies to a rectangular cantilever with a uniform cross section. As can be seen in Fig. 1(a), however, the piezoresistive cantilever is not perfectly rectangular along its entire length and has slotted regions. Detailed calculations that account for the actual geometry of the cantilever, for instance using finite-element analysis, are necessary to determine a more precise value of ζ .

Inserting Eqs. (3)–(5) into Eq. (2), the spring constant k_{piezo} can be determined from the experimentally measured quantities by

$$k_{\text{piezo}} = \frac{S \zeta \Delta V_P \cos^2 \theta}{\delta_T - \frac{S \Delta V_P}{\zeta^2 k_P}}. \quad (7)$$

For each experimental data set, the values of $F \cos \theta = S \zeta \Delta V_P \cos \theta$ were plotted as a function of $\delta_C / \cos \theta = [\delta_T - (S \Delta V_P / \zeta^2 k_P)] / \cos \theta$. An example of the resulting graph is shown in Fig. 5. A linear least-squares fit to all 100 data points was performed, and the slope was taken as the average value of k_{piezo} for the entire data set. (Fitting each of the ten test runs separately and then averaging the

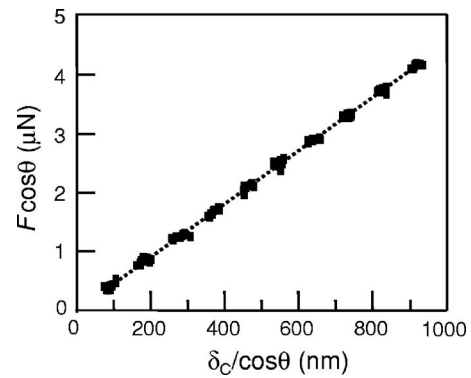


FIG. 5. Example of data analysis to obtain the cantilever spring constant k_C . The individual data points represent the 100 experimental values measured for cantilever no. 2 in a series of ten test runs. The dotted line shows the linear least-squares fit to all of the data, with a slope that corresponds to $k_C = 4.50 \pm 0.07 \text{ N/m}$.

individual slopes produced nearly identical values of the average k_{piezo} .) The method used to determine the measurement uncertainty in k_{piezo} is described in the Appendix. In brief, we calculated error bars for $\delta_C / \cos \theta$ and $F \cos \theta$ based on standard uncertainty analysis. The line-fitting algorithm to determine k_{piezo} then calculated the uncertainty in k_{piezo} based on these error bars.

IV. SPRING-CONSTANT MEASUREMENTS WITH OTHER TECHNIQUES

The spring-constant values obtained with the piezosensor were compared to those measured by four other techniques: (1) the thermal noise method; (2) the Sader method; (3) force calibration with a calibrated nanoindentation instrument; and (4) direct calibration by the EFB. Several other approaches for spring-constant calibration have also been demonstrated. For an overview of different methods, see, for instance, Ref. 17. Because the methods have been discussed in detail elsewhere, they are only briefly described here. The four methods that we used can be grouped into two categories: dynamic methods and force-loading methods. Dynamic methods, such as the Sader method and the thermal noise method, make use of information about the resonant behavior of the cantilever to determine k_C . The remaining techniques—piezosensor, nanoindentation calibration, and EFB calibration—are force-loading methods. In this case, the relation between an applied quasistatic force and the cantilever deflection is used to determine k_C .

A. Thermal noise method

This approach uses the equipartition theorem to relate the cantilever’s Brownian motion to its spring constant k_{therm} .^{18–22} For these measurements, we used the software package provided with the MFP-3D. The first step in the procedure was to determine the cantilever sensitivity (sometimes called the “optical lever sensitivity”), that is, the relation between the cantilever deflection and the corresponding photodiode voltage. The sensitivity measurements were performed on a piece of polished (100) silicon. Measurements were repeated ten times to obtain an average and uncertainty in the sensitivity. The resulting values were multiplied by the

factor $\chi/\cos \theta$, where θ is the tilt angle of the cantilever. The factor χ converts the cantilever sensitivity measured under loading conditions to its value for free-space vibrations.²¹ The value of χ depends on both the size of the laser spot and its relative location on the cantilever. We developed a methodology to reproducibly position the laser spot at the end of the cantilever. This was achieved by adjusting the spot position until the photodiode voltage fell to a fixed fraction of its maximum value (usually 0.8). Figure 6 in Ref. 21 was then used to determine the value of χ based on the laser spot size (50 μm), the cantilever length l , and the relative photodiode amplitude. Typically, $\chi=1.08$ in these experiments.

Next, the thermal noise software routine was run. In this routine, a spectrum of the vibration amplitude versus frequency was acquired and converted to absolute amplitudes by means of the measured cantilever sensitivity. Next, the user manually identified the first free resonance and set a background noise level. The software then performed a peak fit after subtracting a $1/f$ noise floor. The values of f and Q obtained in the fit were recorded for use with the Sader method (see below). The value of k_C calculated in software from the fit was multiplied by $12/(1.8751)^4=0.9707$ to obtain a final value for k_{therm} . This factor accounted for the fact that only the lowest resonant mode was included in the analysis.¹⁹ Fifteen values of k_C were obtained for each cantilever by repeating the procedure in succession. The 15 values were averaged to obtain an average value of k_{therm} . The measurement uncertainty in k_{therm} included the uncertainty in the cantilever sensitivity measurement as well the scatter in the individual values of k_{therm} .

B. Sader method

This method is derived from an analytical formula for the resonant frequency f of the cantilever's lowest flexural mode in free space.^{16,23} It includes corrections for damping effects if the cantilever vibrates in air or another fluid. In addition to f , the method requires values for the quality factor Q of the free resonance and the cantilever length l and width w . For these calculations, we used the values of f and Q determined in the thermal noise experiments described above. The cantilever dimensions were determined by means of an optical microscope. Digital images of the cantilevers in plan view were acquired and analyzed to obtain l and w . For cantilevers with trapezoidal cross sections, the larger of the two widths was used for w . The values of f , Q , l , and w were used as input data for an online calculator²⁴ to obtain k_{Sader} . We used $\rho=1.005 \text{ kg/m}^3$ for the density of air and $\eta=1.84 \times 10^{-5} \text{ kg/s/m}$ for the viscosity of air at our site.²² The measurement uncertainty for k_{Sader} was determined by varying the input values to the online calculator by the uncertainties in each parameter (f , Q , l , and w), and noting the effect on the calculated value of k_{Sader} .

C. Loading by calibrated nanoindentation instrument

In this method,^{12,25} a sinusoidally varying force is applied to the cantilever tip with a sharp diamond stylus, and the resulting displacement is measured to yield a value k_{NI} for the cantilever spring constant. A Hysitron Triboscope in-

dentor with a cube-corner indenter was used for these experiments. An auxiliary load cell was used to calibrate the force measurements of the indenter. Previous work describes the calibration of this load cell with traceable dead weight forces.²⁶ To avoid uncertainties associated with the contact between the indenter tip and AFM cantilever tip, the test was performed 40 μm from the cantilever tip, as measured by the optical encoders on the indenter stage. The measured spring constant was then corrected by use of a factor similar to ζ^3 in Eq. (6). In this case, l_p in Eq. (6) is replaced with the length of the cantilever under test, and Δl is replaced with the distance between the AFM cantilever tip and the test point (i.e., 40 μm). The uncertainty contribution from the position of the contact between the indenter tip and cantilever under test was doubled from the value used in previous work¹² to reflect this procedural modification. The magnitude of the other uncertainty components remained the same.

D. Direct Loading by EFB

To provide a cross check of the other calibration methods, the test cantilevers were calibrated directly by the EFB primary force standard. The procedure was similar to that described in Sec. II C to measure the stiffness k_p of the piezosensor. A flat-punch platen made of sapphire with a 1 mm diameter was used. The cantilever tips were pressed against the flat punch. Several (four to ten) measurements were made on each cantilever in order to obtain values for the average and standard deviation of k_{EFB} .

V. TEST CANTILEVERS

The spring constants of seven different cantilevers were measured by the five different calibration methods described above. All of the cantilevers were micromachined from single-crystal silicon and contained tips. None of the cantilevers contained reflective coatings. Furthermore, all of the cantilevers possessed a rectangular (i.e., not V-shaped) geometry. The cross section of some cantilevers was rectangular, while others had a trapezoidal cross section. The properties of the cantilevers are summarized in Table I. The table gives the values of the cantilever length l and width w and the values f and Q of the first free resonance. As described above, l and w were measured with an optical microscope, and f and Q were measured with the AFM's thermal noise software. Also included are the nominal values of the spring constant k_{nom} quoted by the manufacturer of each cantilever. The uncertainty or variability in k_{nom} was as large as 100% to 200% in some cases, highlighting the need to measure k_C directly. Note that the nominal spring constants for the cantilevers used in this study varied by a factor of 200, that is, by more than two orders of magnitude.

VI. RESULTS AND DISCUSSION

A. Comparison of results

The experimental results are summarized in Table II and Fig. 6. Both the table and the figure show the spring-constant values determined by each method for each of the seven test cantilevers. In Fig. 6, the gray bars indicate the nominal spring-constant values provided by the manufacturers. It can

TABLE I. Measured properties of the AFM cantilevers used in these experiments. Shown are the length l , the width w , and the frequency f and quality factor Q of the first natural resonance. Also shown are the nominal (vendor) values of the cantilever spring constant k_{nom} and the cross-sectional geometry of each cantilever.

No.	l (μm)	w (μm)	f (KHz)	Q	k_{nom} (N/m)	Cross section
1	536.4 \pm 0.2	60.6 \pm 0.3	8.252 \pm 0.002	31.5 \pm 0.5	0.2 \pm 0.4	Trapezoidal
2	245.4 \pm 0.4	41.0 \pm 0.8	66.542 \pm 0.002	296.6 \pm 4.2	3.5 \pm 0.8	Rectangular
3	247.0 \pm 0.4	43.1 \pm 0.2	70.197 \pm 0.003	268.7 \pm 9.8	3.5 \pm 0.8	Rectangular
4	252.9 \pm 0.2	46.5 \pm 0.2	126.764 \pm 0.002	280.7 \pm 2.6	15 \pm 16	Trapezoidal
5	248.9 \pm 0.4	46.6 \pm 0.5	129.373 \pm 0.003	275.1 \pm 3.3	15 \pm 16	Trapezoidal
6	250.9 \pm 0.4	43.2 \pm 0.1	174.217 \pm 0.002	790 \pm 21	40 \pm 18	Rectangular
7	247.9 \pm 0.4	46.0 \pm 0.2	175.063 \pm 0.002	792 \pm 17	40 \pm 18	Rectangular

be seen that the measured values often differ substantially from the nominal value. For instance, in the case of the most compliant cantilever (no. 1), the nominal value is approximately three times as large as the measured values (0.2 N/m versus \sim 0.06 N/m). Most likely, this discrepancy is due to a difference between the actual and nominal value of the cantilever thickness t . Because k_C scales as t^3 , even a fairly minor difference in thickness has a relatively large effect on k_C in thin, compliant cantilevers. Even for the stiffest cantilevers (nos. 6 and 7), the measured spring constants differ by roughly 25% from the nominal values. This discrepancy illustrates why direct measurements of k_C are critical for applications that require accurate force measurements.

Further examination of Table II and Fig. 6 reveals that in most cases, the values of k_C obtained by the different methods are approximately the same for a given cantilever. This is particularly true for cantilever no. 3. The most obvious exceptions are for the stiffest cantilevers (nos. 6 and 7). Although the values of k_{Sader} , k_{NI} , and k_{EFB} for these cantilevers are nearly identical within measurement uncertainty, the thermal noise method overestimates k_C by \sim 20% to 25%. We believe that this is due to poor signal-to-noise ratios. As the cantilever stiffness increases, the vibration amplitude of thermal fluctuations decreases relative to the $1/f$ noise floor. Thus, the thermal noise calculation becomes highly sensitive to the noise level used in the peak fitting software. This effect may also explain the somewhat high value of k_{therm} for cantilever no. 5 and the somewhat low value for cantilever no. 4.

In addition, the spring constant values for cantilevers nos. 6 and 7 obtained with the piezosensor are \sim 10%–15%

higher than those obtained by the Sader, nanoindentation, and EFB methods. One possible explanation is that the stiffness k_p of the piezoresistive cantilever is roughly 1/20 the stiffness of those cantilevers. It is a general rule of thumb for reference cantilever methods that the stiffness of the test and reference cantilevers should be roughly the same.¹⁷ Another possible explanation why the values of k_{piezo} for cantilevers nos. 6 and 7 are higher than the other measured values concerns the tip location coefficient ζ . As discussed above, ζ is determined by the geometry of the piezoresistive cantilever, so that the true value may differ from the assumed value of 1.041. Table III shows how changes in ζ affect k_{piezo} . For test cantilevers with stiffness less than or approximately the same as the stiffness of the piezoresistive cantilever (nos. 1–3), small changes in ζ have very little effect on k_{piezo} . The effect of ζ on k_{piezo} increases as the stiffness of the test cantilever increases. For the stiffest cantilevers, with $k_{\text{piezo}} \approx 50$ N/m (nos. 6 and 7), changing ζ from 1.041 to 1.047 decreases k_{piezo} by approximately 15%–20%, and results in values smaller than the other measurements.

From these results, the overall accuracy of the piezosensor method can be assessed. We omit the results for cantilevers nos. 6 and 7 and judge only the results for cantilevers nos. 1–5. Comparing the values of k_{piezo} to the average values for each cantilever, we conclude that the piezosensor transfer standard yields values for k_C that are accurate to $\pm 5\%$ to $\pm 10\%$. It is important to note that this statement applies to cantilevers with spring constants that vary by more than two orders of magnitude (\sim 0.06 N/m to \sim 12 N/m).

TABLE II. Measured cantilever spring constant values (in N/m) obtained by five methods: calibrated piezosensor (k_{piezo}), thermal method (k_{therm}), Sader method (k_{Sader}), calibrated nanoindentation (k_{NI}), and direct calibration with the EFB (k_{EFB}). The nominal spring constant (k_{nom}) specified by the vendor is also included for comparison. In cases where a value is not given, the cantilever broke during measurement.

	Cantilever no.						
	1	2	3	4	5	6	7
k_{nom}	0.2 \pm 0.4	3.5 \pm 0.8	3.5 \pm 0.8	15 \pm 16	15 \pm 16	40 \pm 18	40 \pm 18
k_{piezo}	0.0667 \pm 0.0010	4.50 \pm 0.07	4.86 \pm 0.07	12.2 \pm 0.6	12.4 \pm 0.6	56.9 \pm 6.6	59.8 \pm 7.0
k_{therm}	0.0652 \pm 0.0027	4.24 \pm 0.06	4.81 \pm 0.15	9.2 \pm 0.2	14.1 \pm 0.2	61.9 \pm 1.3	64.7 \pm 1.5
k_{Sader}	0.0694 \pm 0.0011	4.12 \pm 0.09	4.24 \pm 0.16	11.5 \pm 0.1	11.4 \pm 0.2	47.8 \pm 1.3	50.7 \pm 1.1
k_{NI}	4.59 \pm 0.24	9.2 \pm 0.4	11.8 \pm 0.5	49.7 \pm 2.0	54.8 \pm 2.2
k_{EFB}	0.0634 \pm 0.0007	3.68 \pm 0.01	4.38 \pm 0.02	11.2 \pm 0.3	...	49.2 \pm 0.5	53.4 \pm 1.0

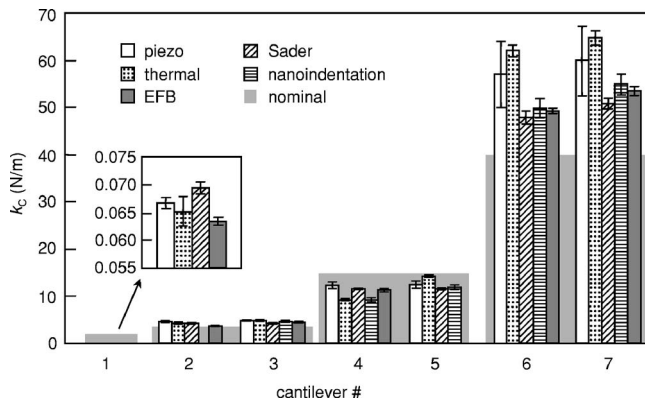


FIG. 6. Comparison of results obtained for k_C by five different methods: calibrated piezosensor, Sader, thermal noise, force loading with a calibrated nanoindentation instrument, and direct calibration on the NIST electrostatic force balance (EFB). The gray areas indicate the nominal value k_{nom} provided by the manufacturer for each cantilever.

B. Relative merits of the piezosensor method

The piezosensor method possesses several attractive features. Most significant is the fact that it provides a force standard traceable to SI units. Like other force-loading methods, the calibration is performed in the same manner in which the cantilever will be used, namely, with the force applied to the tip. Furthermore, the method does not depend on cantilever geometry and can be applied to cantilevers with tips. This approach also does not require supplemental measurements of cantilever dimensions with optical or electron microscopy, unlike some other methods. As discussed above, a single piezosensor provides accurate measurements for cantilevers with a wide range of stiffnesses.

One of the most notable advantages of the piezosensor method is that it does not involve the AFM's photodiode signal. Accurate, repeatable calibration of the photodiode sensitivity can be difficult, partly because the response is not linear over the entire range.^{13,14} Furthermore, the photodiode sensitivity must be measured for each new experimental configuration, that is, the current location of the laser spot on the cantilever.²¹ Because the piezosensor provides an active readout of voltage versus force, both its force and deflection can be determined without the photodiode signal. Our method makes use of a separate sensor (Z-LVDT) to determine the motion of the AFM head. If no such sensor is available, the z -scanner can be calibrated by other means, for instance with a nanoindentation load cell⁹ or with the piezoresistive cantilever itself.

The piezosensor method also possesses disadvantages,

most of which are shared by other reference cantilever methods. As discussed in the Appendix, the measurement uncertainty increases strongly as the spring constant ratio k_C/k_P increases. One single reference cantilever therefore should not be used to calibrate all AFM cantilevers. In addition, like any force-loading method, the piezosensor approach can potentially damage the tip of the test cantilever. All force-loading methods also require precise knowledge of the tip position. The value of k_P was calibrated for a specific loading position, and will change if the position varies. This is the reason why a procedure was developed to locate a reliable tip position, and why the factor ζ was included. As discussed above, k_{piezo} is sensitive to relatively small uncertainties in ζ that occur either from slight variations in the loading position or from uncertainty in the true value of ζ . Moreover, the sensitivity increases as the cantilever stiffness ratio k_C/k_P increases. In hindsight, the correction factor ζ could be eliminated by removing a small portion of the tip prior to calibration by the EFB. Creating a flat region on the tip would ensure that subsequent calibrations of test cantilevers are performed at the same spot as the EFB measurements.

In summary, we have described a method to measure the spring constant k_C of AFM cantilevers by means of a piezosensor containing a piezoresistive cantilever. When calibrated by the NIST EFB force standard, the piezoresistive cantilever and its readout electronics form a piezosensor force transfer standard that is traceable to SI units. We used the piezosensor method to measure seven AFM cantilevers with nominal spring constants from 0.2–40 N/m. The values of k_C measured by the piezosensor technique were compared to those obtained by four other methods. When the compliance of the test cantilever is comparable to, or less than, that of the piezoresistive cantilever, the piezosensor force transfer standard provides values of k_C that are accurate to $\pm 5\%$ to $\pm 10\%$. The piezosensor approach has the advantages that it can be used regardless of cantilever geometry, eliminates the need to calibrate the AFM photodiode detector, and mimics the loading conditions under which the cantilever will be used. By enabling more accurate measurements of forces, calibration methods such as this will improve our ability to extract quantitative information from AFM methods.

ACKNOWLEDGMENTS

We thank R. Geiss (NIST) for providing SEM images of the piezoresistive cantilever, and P. Rice (NIST and University of Colorado) for performing initial calibrations of the

TABLE III. Effect of the value of the tip location coefficient ζ on the spring constant k_{piezo} determined with the piezosensor method. For comparison, the value k_{EFB} measured with the EFB is shown. All of the spring constants are given in units of N/m.

	Cantilever no.						
	1	2	3	4	5	6	7
$k_{\text{piezo}} (\zeta=1.041)$	0.0667 ± 0.0010	4.50 ± 0.07	4.86 ± 0.07	12.2 ± 0.6	12.4 ± 0.6	56.9 ± 6.6	59.8 ± 7.0
k_{EFB}	0.0632 ± 0.0008	3.44 ± 0.03	4.38 ± 0.02	11.3 ± 0.2	...	49.2 ± 0.6	53.4 ± 1.0
$k_{\text{piezo}} (\zeta=1.047)$	0.0670 ± 0.0010	4.46 ± 0.07	4.81 ± 0.07	11.8 ± 0.5	12.0 ± 0.6	48.1 ± 5.1	50.1 ± 5.3

piezosensor. This is a contribution of NIST, an agency of the U.S. government; not subject to copyright.

APPENDIX: UNCERTAINTY ANALYSIS

Here, we derive the uncertainty in the cantilever spring constant k_{piezo} measured with the piezosensor method. k_{piezo} is determined by a fit to the line $y = k_{\text{piezo}} x$, where

$$x = \frac{\delta_C}{\cos \theta} = \frac{\delta_T - \frac{S\Delta V_P}{\zeta^2 k_P}}{\cos \theta} \quad (\text{A1})$$

and

$$y = F \cos \theta = S\zeta\Delta V_P \cos \theta. \quad (\text{A2})$$

For a given variable $y = f(x_1, x_2, x_3, \dots)$, the combined standard uncertainty $U_c(y)$ in y is given by²⁷

$$U_c^2(y) = \sum_{i=1}^N \left(\frac{\partial f}{\partial x_i} \right)^2 U^2(x_i) + 2 \sum_{i=1}^{N-1} \sum_{j=i+1}^N \frac{\partial f}{\partial x_i} \frac{\partial f}{\partial x_j} U(x_i, x_j). \quad (\text{A3})$$

For these measurements, we assume that all of the variables x_i ($\delta_T, S, \Delta V_P, \zeta, k_P, \theta$) are uncorrelated, so that the second term in Eq. (A3) vanishes.

The sensitivity coefficients $\partial f / \partial x_i$ are determined from the partial derivatives of Eqs. (A2) and (A1). For Eq. (A1) with $x = f_1(\delta_T, S, \Delta V_P, \zeta, k_P, \theta)$,

$$\frac{\partial f_1}{\partial \delta_T} = \frac{1}{\cos \theta}, \quad (\text{A4})$$

$$\frac{\partial f_1}{\partial S} = \frac{-\Delta V_P}{\zeta^2 k_P \cos \theta}, \quad (\text{A5})$$

$$\frac{\partial f_1}{\partial \Delta V_P} = \frac{-S}{\zeta^2 k_P \cos \theta}, \quad (\text{A6})$$

$$\frac{\partial f_1}{\partial \zeta} = \frac{2S\Delta V_P}{\zeta^3 k_P \cos \theta}, \quad (\text{A7})$$

$$\frac{\partial f_1}{\partial k_P} = \frac{S\Delta V_P}{\zeta^2 k_P^2 \cos \theta}, \quad (\text{A8})$$

and

$$\frac{\partial f_1}{\partial \theta} = \left(\delta_T - \frac{S\Delta V_P}{\zeta^2 k_P} \right) \frac{\sin \theta}{\cos^2 \theta}. \quad (\text{A9})$$

The combined relative uncertainty $U_{c,r}(x)$ in x is therefore

$$U_{c,r}^2(x) = \frac{U_c^2(x)}{x^2} = \left(\frac{k_C}{k_P} \right)^2 \left[\frac{U^2(S)}{S^2} + \frac{U^2(\Delta V_P)}{\Delta V_P^2} + \frac{U^2(k_P)}{k_P^2} + 4 \frac{U^2(\zeta)}{\zeta^2} \right] + \frac{U^2(\delta_T)}{\delta_C^2} + U^2(\theta) \tan^2 \theta. \quad (\text{A10})$$

Here, we have used

$$\frac{k_C}{k_P} = \frac{S\zeta\Delta V_P}{\zeta^3 k_P \left(\delta_T - \frac{S\zeta\Delta V_P}{\zeta^2 k_P} \right)} = \frac{S\Delta V_P}{\zeta^2 k_P \left(\delta_T - \frac{S\Delta V_P}{\zeta^2 k_P} \right)}, \quad (\text{A11})$$

where k_C/k_P is the stiffness k_C of the cantilever under test relative to that of the piezosensor k_P .

Equation (A10) reveals that the relative cantilever stiffness k_C/k_P strongly affects the measurement uncertainty in the cantilever displacement δ_C . For $k_C > k_P$, the uncertainty rapidly increases with increasing compliance mismatch. This is one justification for the general rule of thumb that the stiffness of the test and reference cantilevers should be roughly the same.¹⁷ Interestingly, note that for $k_C < k_P$, the uncertainty actually decreases.

For Eq. (A2) with $y = f_2(S, \Delta V_P, \theta, \zeta)$,

$$\frac{\partial f_2}{\partial S} = \zeta \Delta V_P \cos \theta, \quad (\text{A12})$$

$$\frac{\partial f_2}{\partial \Delta V_P} = S\zeta \cos \theta, \quad (\text{A13})$$

$$\frac{\partial f_2}{\partial \theta} = -S\zeta \Delta V_P \sin \theta, \quad (\text{A14})$$

and

$$\frac{\partial f_2}{\partial \zeta} = -S\Delta V_P \cos \theta. \quad (\text{A15})$$

The combined relative uncertainty $U_{c,r}(y)$ in y is therefore

$$U_{c,r}^2(y) = \frac{U_c^2(y)}{y^2} = \frac{U^2(S)}{S^2} + \frac{U^2(\Delta V_P)}{\Delta V_P^2} + U^2(\theta) \tan^2 \theta + \frac{U^2(\zeta)}{\zeta^2}. \quad (\text{A16})$$

To calculate the measurement uncertainty in k_{piezo} , we used Eqs. (A10) and (A16) to generate error bars in both x ($\delta_C / \cos \theta$) and y ($F \cos \theta$) for each data point. All of the data points for a given cantilever were fit to a single line in order to calculate the average slope, that is, k_{piezo} . The line-fitting algorithm also analyzed the measurement uncertainties in x and y to determine the uncertainty in k_{piezo} ;²⁸ these are the values quoted in Table II. For these calculations, we used $U(S)/S = 0.14/24.58 = 0.006$, $U(\Delta V_P) = 0.002$ V, $U(\theta) = 0.2^\circ$, $U(\delta_T) = 30$ nm, $U(k_P)/k_P = 0.10/3.10 = 0.03$, and $U(\zeta)/\zeta = 0.004/1.041 = 0.004$. For the value k_C in the ratio k_C/k_P , we used the nominal spring constant for each type of cantilever (k_{nom} in Table I).

¹H.-J. Butt, B. Cappella, and M. Kappl, Surf. Sci. Rep. **59**, 1 (2005).

²A. Torii, M. Sasaki, K. Hane, and S. Okuma, Meas. Sci. Technol. **7**, 179 (1996).

³C. T. Gibson, G. S. Watson, and S. Myhra, Nanotechnology **7**, 259 (1996).

⁴M. Tortonesi and M. D. Kirk, Proc. SPIE **3009**, 53 (1997).

⁵P. J. Cumpson, C. A. Clifford, and J. Hedley, Meas. Sci. Technol. **15**, 1337 (2004).

⁶R. S. Gates and J. R. Pratt, Meas. Sci. Technol. **17**, 2852 (2006).

⁷I. Behrens, L. Doerig, and E. Peiner, J. Micromech. Microeng. **13**, S171 (2003).

⁸G. A. Matei, E. J. Thoreson, J. R. Pratt, D. B. Newell, and N. A. Burnham, Rev. Sci. Instrum. **77**, 083703 (2006).

⁹S. B. Aksu and J. A. Turner, Rev. Sci. Instrum. **78**, 043704 (2007).

¹⁰Commercial equipment and materials are identified only in order to adequately specify certain procedures. In no case does such identification imply recommendation or endorsement by the National Institute of Standards and Technology, nor does it imply that the materials or equipment identified are necessarily the best available for the purpose.

¹¹J. R. Pratt, J. A. Kramar, D. B. Newell, and D. T. Smith, Meas. Sci. Technol. **16**, 2129 (2005).

- ¹²G. A. Shaw, J. Kramar, and J. Pratt, *Exp. Mech.* **47**, 143 (2007).
- ¹³T. E. Schäffer, *J. Appl. Phys.* **91**, 4739 (2002).
- ¹⁴E. C. C. M. Silva and K. J. Van Vliet, *Nanotechnology* **17**, 5525 (2006).
- ¹⁵J. L. Hutter, *Langmuir* **21**, 2630 (2005).
- ¹⁶J. E. Sader, I. Larson, P. Mulvaney, and L. R. White, *Rev. Sci. Instrum.* **66**, 3789 (1995).
- ¹⁷B. Ohler, "Practical Advice on the Determination of Cantilever Spring Constants," Veeco Application Note, available at www.veeco.com/library/appnotes.php?page=category&category_id=1 (accessed July 2007).
- ¹⁸J. L. Hutter and J. Bechhoefer, *Rev. Sci. Instrum.* **64**, 1868 (1993).
- ¹⁹H.-J. Butt and M. Jaschke, *Nanotechnology* **6**, 1 (1995).
- ²⁰N. A. Burnham, X. Chen, C. S. Hodges, G. A. Matei, E. J. Thoreson, C. J. Roberts, M. C. Davies, and S. J. B. Tandler, *Nanotechnology* **14**, 1 (2003).
- ²¹R. Proksch, T. E. Schäffer, J. P. Cleveland, R. C. Callahan, and M. B. Viani, *Nanotechnology* **15**, 1344 (2004).
- ²²S. M. Cook, T. E. Schäffer, K. M. Chynoweth, M. Wigton, R. W. Simmonds, and K. M. Lang, *Nanotechnology* **17**, 2135 (2006).
- ²³J. E. Sader, J. W. M. Chon, and P. Mulvaney, *Rev. Sci. Instrum.* **70**, 3967 (1999).
- ²⁴www.ampc.ms.unimelb.edu.au/afm (accessed July 2007).
- ²⁵J. D. Holbery, V. L. Eden, M. Sarikaya, and R. M. Fisher, *Rev. Sci. Instrum.* **71**, 3769 (2000).
- ²⁶R. A. Seugling and J. R. Pratt, in *Proceedings of the ASPE Annual Meeting*, Orlando, FL (2004).
- ²⁷B. N. Taylor and C. E. Kuyatt, "Guidelines for Evaluating and Expressing the Uncertainty of NIST Measurement Results," NIST Technical Note 1297 (1994); available at <http://physics.nist.gov/Pubs/pdf.html> (accessed July 2007).
- ²⁸W. H. Press, S. A. Teukolsky, W. T. Vetterling, and B. P. Flannery, *Numerical Recipes in FORTRAN: The Art of Scientific Computing*, 2nd ed. (Cambridge University Press, Cambridge, 1992), p. 660.